https://doi.org/10.1016/j.still.2021.105083

A new simple and low-cost air permeameter for measuring air permeability of unsaturated soil

Rui Chen[a,b], Jun-Wen Huang[b], Chao Zhou[c], Yang Ping[d], Zhong-Kui Chen[b,*]

[a]*Shenzhen Key Laboratory of Smart Structural System in Civil Engineering, Harbin Institute of Technology, Shenzhen, China*

[b]*School of Civil and Environmental Engineering, Harbin Institute of Technology, Shenzhen, China*

[c]*Department of Civil and Environmental Engineering, Hong Kong Polytechnic University, Hung Hom, Kowloon, Hong Kong, China*

[d]*PowerChina Eco-Environmental Group Co., LTD., China*

Abstract

Air permeability, k_a, plays an important role in understanding air transport behavior in unsaturated soils. As for the measurement of k_a, existing air permeameters using steady-state methods are relatively complicated and costly. Therefore, in this study, a new simple and low-cost air permeameter was developed, which can supply steady air pressure on soil specimen and measure the flow rate of air through soil specimen accurately. To verify the reliability of measurement results using this new air permeameter, a comparison of measured k_a of clay, silt loam, and sandy loam specimens between the new air permeameter and the one proposed in ASTM D6539 was conducted. One-way analysis of variance shows that the difference of measured k_a of soil specimen between the two air permeameters is not significant (p >0.05).

Keywords

Air permeability; Air permeameter; Unsaturated soil; Air pressure; Flow rate

1. Introduction

Air permeability of unsaturated soils, k_a, is of great concern in agriculture where soil aeration is essential for plant growth (Gliński and Stępniewski, 1985; Chen et al., 2019; Wang et al., 2021). Moreover, k_a can be used to predict soil hydraulic permeability which is also an essential soil parameter (Iversen et al., 2003; Rahmati et al., 2019; Chen et al., 2021;).

Air permeability of unsaturated soils can be measured directly by transient methods or steady-state methods. As for the transient methods, the gradient of air pressure along the length of soil specimen decreases during measurement (e.g., Delage et al., 1998; Meyer et al., 2014). As for the steady-state methods, the gradient of air pressure along the length of soil specimen is maintained constant during

measurement (e.g., ASTM, 2013; Ni et al., 2019；Peng et al., 2020；Zhan et al., 2020). Since the density of air strongly depends on its pressure, the decrease of air pressure in the transient method would lead to a decrease of air density, thereby causing inaccurate measurement of the volumetric flow rate of air through soil specimen. Therefore, steady-state methods are more preferred than transient methods.

However, existing air permeameters using steady-state methods are relatively complicated and costly. For example, when an air compressor is used as an air source for air permeameter, because the air compressor usually supplies compressed air with greatly varying air pressure, at least two high-quality air pressure regulators are needed to provide steady air pressure to soil specimen (Zhan et al., 2014; Kosmaras, 2017; Qiu et al., 2021). Moreover, air pressure right on the top and bottom of soil specimen is usually needed to be measured (e.g., ASTM, 2013), but the standard tri-axial cell is not suitable for measurement of air pressure right on the top and bottom of soil specimen unless modification is conducted.

In this study, a new simple and low-cost air permeameter for the steady-state method was developed. To verify the reliability of measurement results obtained from this new permeameter, k_a of soil specimens with three soil textures, i.e., clay, silt loam, and sandy loam were measured using both this new air permeameter and the air permeameter specified by ASTM D6539 (ASTM, 2013). Then the measured results from the two air permeameters were compared and discussed.

2. Material and methods

2.1 A new simple and low-cost air permeameter

Fig. 1 and Fig. 2 show schematic diagram and photograph of the newly developed air permeameter, respectively. The new air permeameter consists of an air

supply system, a permeameter cell, and a water pressure source. The air supply system mainly contains two bottles: bottle A and bottle B. Each bottle has an inner diameter of 18 cm and a height of 28 cm. Bottle A is a Mariotte's bottle which is connected to bottle B by a water pipe. Bottle B is a reversed Mariotte's bottle. Moreover, air pressure in bottle B (P_B) is monitored by a U-shaped tube filled with water with an accuracy of 0.01 kPa. Change of water level in bottle B can be measured by a paper ruler attached to bottle B with an accuracy of 1 mm. Reading of the paper ruler can be monitored in real-time by a webcam. Bottle B and a standard triaxial cell which acts as a permeameter cell are linked by an air pipe. The space between the outer wall and soil specimen in the standard triaxial cell is filled with water.

When bottle A is placed to a relatively higher elevation than bottle B, a steady water pressure (P_w) is generated. When air pressure in bottle B (P_B) is smaller than P_w, water in bottle A flows into bottle B through a water pipe. An increase in the volume of water in bottle B results in compression of air in bottle B and thus P_B increases. The compressed air with the air pressure of P_B is connected to the bottom of the soil specimen through an air pipe. Meanwhile, the top of the soil specimen is directly connected to the atmosphere (P_0). The difference in air pressure between the bottom and the top of the soil specimen drives the transport of air through the soil specimen.

Bottle B also plays a role to measure the volumetric flow rate of air at the air pressure of P_B. When the dynamic equilibrium between out-flow of air and in-flow of water in bottle B is achieved, the volume of water flowing into bottle B is equal to the volume of air at the air pressure of P_B flowing out from bottle B within a given time interval (Δt). Therefore, the volumetric flow rate of air (q_B) at the air pressure of P_B can be measured indirectly by measuring the volumetric flow rate of water. The flow

rate of water can be obtained conveniently and accurately by measuring the change of water level in bottle B within Δt, i.e. Δh_w. Then the volume of water flowing into bottle B can be obtained from the product of the cross-sectional area of bottle B (A') and Δh_w.

Components of the new air permeameter and the air permeameter using the backpressure control method introduced in ASTM D6539 (ASTM, 2013) are listed in Table 1. From this table, it was found that the new air permeameter developed in this study is simpler in structure and low cost as compared with the air permeameter introduced in ASTM D6539. For the air permeameter introduced in ASTM D6539, to satisfy the requirement of measurement of air permeability, an air compressor, two or more air pressure regulators, an air flowmeter with good precision, an air pressure transducer, and a differential pressure transducer with good precision are required. However, the new air permeameter developed in this study consists of fewer and simpler components, namely two Marriote's bottles, a U-shaped tube, and a paper ruler. Moreover, unlike the air permeameter of ASTM D6539 which requires a custom-made tri-axial cell, the new air permeameter in this study only needs a standard triaxial cell.

2.2 Test procedure for measuring k_a

Prior to the test, a leak check was performed to determine gas tightness. Firstly, the inlet valve of the triaxial cell was closed and then bottle A was set to an elevation that was higher than that of bottle B. If no water flowed into bottle B and no change of water level in the U-shaped tube occurred, it could be regarded that the air supply system had good sealing. After leak check, soil specimen wrapped around by a rubber membrane, i.e. flexible wall, was placed in the standard triaxial cell. To prevent

111 preferential flow along the sidewall of the soil specimen during the test, a low
112 confining pressure which was about 15 kPa larger than P_B was applied on the soil
113 specimen by a water pressure source. After that, the ambient temperature and the
114 barometric pressure were recorded. Then the inlet and the outlet valves of the triaxial
115 cell were opened and thus compressed air stored in bottle B started to flow through
116 the soil specimen. When the reading of the U-shaped tube (i.e. P_B) was stable, the
117 permeability test started. During the test, the readings of the U-shaped tube and paper
118 ruler were monitored. The test was ended when water elevation in bottle B increased
119 by 5 mm. Then the above procedure was repeated when bottle A was placed at
120 another two elevations higher than that of bottle B. The average of three k_a
121 corresponding to three elevations of bottle A was regarded as the representative k_a of
122 the soil specimen. Moreover, all the experiments were performed in a
123 temperature-controlled room (i.e., 20±1℃).

124 *2.3 Calculation of k_a*

125 The process of calculation of k_a is similar to Ye et al. (2009). During the air
126 permeability test, soil specimen with a height of L (m) is under the following
127 boundary conditions: the top and the bottom of soil specimen are under uniform air
128 pressure of P_0 (Pa) and P_B (Pa), respectively. P_0 is the absolute pressure of barometric
129 air pressure, i.e. P_0= 1 atm. P_B is the absolute air pressure in bottle B. Thus pressure
130 drop across the specimen (ΔP) is the difference between P_B and P_0.

131 As for an infinitesimal soil layer with a thickness of dx (m) at a height of x in the
132 vertical coordinate, the volumetric flow rate of air through the infinitesimal soil layer
133 at the height of x, i.e., $q(x)$ ($m^3\ s^{-1}$), can be expressed by Darcy's law:

134 $$q(x) = \frac{-K \times A \times dP(x)}{\mu_a \times dx} \quad (1)$$

where K (m^2) is intrinsic permeability; A (m^2) is the cross-sectional area of soil specimen; μ_a is the dynamic viscosity of air (P_a·s). Because μ_a depends mostly on temperature (Montgomery, 1947) and permeability tests in this study were conducted indoors, the room temperature was stable and μ_a can be regarded as a constant in this study; $P(x)$ (P_a) is the air pressure at height of x.

Multiplying $P(x)$ on both sides of Equation (1) yields:

$$P(x)\times q(x)=-\frac{K\times A\times P(x)\times dP(x)}{\mu_a\times dx} \tag{2}$$

When the flow of air through soil specimens is stable, the amount of air molecule (n (mole)) which flows through any section of soil specimen at a given time interval Δt (s) is assumed to be identical. Thus following equation can be obtained based on Boyle's law:

$$P(x)\times q(x)=P_{\mathrm{B}}\times q_{\mathrm{B}}=\frac{n\times R\times T}{\Delta t} \tag{3}$$

where R is the ideal gas constant; T (K) is the absolute temperature. q_B ($m^3\ s^{-1}$) is the volumetric flow rate of air at an air pressure of P_B. Because q_B is equal to the volumetric flow rate of water in this study, q_B can be calculated by the following equation:

$$q_{\mathrm{B}}=\frac{A'\times(\Delta h_w)}{\Delta t} \tag{4}$$

where A'(m^2) is the cross-sectional area of water in bottle B; Δh_w (m) is the change of difference of water level in bottle B at time interval Δt (s).

According to Equation (3), replacing $P(x)\times q(x)$ with $P_{\mathrm{B}}\times q_{\mathrm{B}}$ in Equation (2) and integrating both sides yields:

$$P_{\mathrm{B}}\times q_{\mathrm{B}}\times L=(-\frac{K\times A}{2\mu_a})\times(P_0^{\ 2}-P_{\mathrm{B}}^{\ 2}) \tag{5}$$

157 Thus expression of K can be obtained from Equation (5). Note that both P_0 and
158 P_B are absolute pressure:

159 $$K = \frac{2\mu_a \times P_B \times q_B \times L}{(P_B^2 - P_0^2) \times A} \quad (6)$$

160 According to the relationship between K and k_a (m s^{-1}) (Carman, 1956), the
161 expression of k_a under air pressure of $P(x)$ can be obtained:

162 $$k_a(P(x)) = \frac{K \times \rho_a(P(x)) \times g}{\mu_a} \quad (7)$$

163 In this study, the k_a under average air pressure of soil specimen
164 namely $P(x) = P_{av} = \frac{P_0 + P_B}{2}$ is selected to represent the k_a of the whole soil specimen.

165 Besides, according to equation (3), the average volumetric flow rate of air at P_{av}
166 during the test, i.e., q_{av} (m^3 s^{-1}) can be calculated by the following equation:

167 $$q_{av} = \frac{q_B \times P_B}{P_{av}} \quad (8)$$

168 *2.4 Soil properties*

169 Three types of soil were used in this study, i.e. completely decomposed granite,
170 silt and a type of kaolin from China. The completely decomposed granite is widely
171 distributed in South China (Chen et al., 2020). The silt is a mixture of quartz sand,
172 quartz powder (Ng et al., 2015b). According to the United States Department of
173 Agriculture (USDA) soil classification system (USDA-NRCS, 2019), the three soils
174 are classified as sandy loam, silt loam and clay, respectively. Reference dry bulk
175 density represents the effect of loading of farm vehicles on the soil after normal field
176 treatments (Håkansson, 1990). According to Håkansson (1990), the reference dry bulk
177 densities of the three soils are obtained by conducting a drained, uniaxial compression
178 test in which a stress of 200 kPa was applied on wet and loose soil. The physical

properties of the three soils are summarized in Table 2.

2.5 Preparation of test specimens

The three soils were first dried in an oven at a temperature of about 105℃. Subsequently, the dry soil was crushed with a rubber hammer and then well mixed with water to its optimum gravimetric water content, i.e., 0.19, 0.16, and 0.36 for sandy loam specimen, silt loam specimen, and clay specimen, respectively. Aggregates of wet silt loam and wet clay were broken by hand so that they were able to pass through a 2-mm sieve (Ng et al., 2015a). The wet sandy loam was also sieved (<5 mm) (Chen et al., 2020). Then mixed wet soil was kept in a zipped plastic bag for five days to reach moisture equilibrium. Thereafter, the soil was compacted in a cylindrical compaction mold to form soil specimen 62 mm in diameter and 100 mm in height. To simulate the effect of loading of farm vehicles on soil, the soil was compacted to its reference dry bulk density. The soil was compacted in five layers with each sublayer of 20 mm thickness. The interface between the two layers was scarified to achieve uniformity. To ensure the repeatability of the experimental results, three replicates for each soil were prepared. For each soil, the three replicates were utilized to perform the permeability tests.

2.6 Measurement of soil air permeability by the method of ASTM D6539

As for the air permeameter of ASTM D6539, air supply system consists of one air compressor (750W-30L, Outstanding, China) linked to two air pressure regulators (IR2000-02BG, SMC, Japan). Air flow rate is measured by an electronic flowmeter with a measuring range from 0 to10 L/min (MF5706-N-10, Siargo, USA). A differential air pressure transducer and an air pressure transducer are connected to a

202 custom-made triaxial cell, aiming to measure air pressure drop across the soil
203 specimen, i.e. ΔP (Pa) and air pressure right on the bottom of soil specimen, i.e.
204 P_{bottom} (Pa). The average volumetric flow rate of air at the average pressure during the
205 test (q_{av}, m^3 s^{-1}) and K for the method of ASTM D6539 are calculated according to
206 equations introduced in ASTM (2013). The air permeability (i.e. k_a) is calculated
207 according to equation (7) and the value of $P(x)$ is selected as the average of P_0 and P_B
208 which are obtained from the test using the new air permeameter.

209 *2.7 Statistical analysis*

210 One-way analysis of variance (ANOVA) was carried out to determine significant
211 difference between k_a of soil specimen measured by new air permeameter and k_a
212 measured by air permeameter of ASTM D6539. The one-way ANOVA was carried out
213 with SPSS 21 (SPSS Inc., Chicago, IL, USA) at the 95% confidence level.

214 **3. Results and discussion**

215 Fig. 3 shows q_{av} at different ΔP during measurement of soil air permeability by
216 the air permeameter introduced in ASTM D6539 and by the new air permeameter of
217 this study. Measured points of each soil specimen were fitted by linear function with
218 intercept fixed to zero. Data of empty points and solid points are measured by the new
219 air permeameter and the air permeameter of ASTM D6539, respectively. Moreover,
220 the measured data at a lower pressure range (i.e., less than 3 kPa) is enlarged in Fig. 3.
221 As shown in Fig. 3, measured points from both two air permeameters locate very
222 close to the best-fit lines, indicating that the measured results conform to Darcy's law.

223 Fig. 4 shows measured k_a of clay, silt loam, and sandy loam specimens by the
224 new air permeameter of this study and by the air permeameter of ASTM D6539. Error
225 bars indicate standard errors of the three replicates. It is found that measured k_a by the

new air permeameter is close to that of the air permeameter of ASTM D6539. Moreover, the results of ANOVA (Table 3) show that the difference of measured k_a of clay, silt loam, and sandy loam specimens between the new air permeameter and the air permeameter of ASTM D6539 is not significant (p >0.05). This clearly demonstrates that measured k_a using the new air permeameter is reliable.

It should be noted that measured k_a of clay specimen is the largest, followed by that of silt loam specimen and then sandy loam specimen (as shown in Fig. 4). This observation seems contradictory to the common sense that a soil with higher clay content should have lower permeability than the one with lower clay content. The contradiction is likely because soil specimens used in this study are repacked soil. To obtain repacked soil specimens, dry soil powder was mixed with water to reach the target gravimetric water content and then the wet soil was compacted into a repacked specimen. During the mixing process of dry soil and water, large-sized aggregates would be formed if the soil has relatively high clay content (Thom et al, 2007; Zhan et al., 2014). Forming of the aggregates would lead to a decrease of the specific surface area of the soil, i.e., the total surface area per unit of soil mass. In this study, the diameter of the aggregate of soil with 60% clay content was controlled to be about 2 mm which is close to the diameter of very coarse sand particles. Hence, inter-aggregate pores (i.e., large pores between soil aggregates) can be formed in clay specimen (Thom et al, 2007). Fig.4 also shows that more large pores were found on the surface of clay specimen than that of silt loam specimen and sandy loam specimen. Since large pore is the main channel for the transport of fluid in soil (Beven and Germann, 1982), k_a of clay specimen is larger than that of silt loam specimen and sandy loam specimen. Furthermore, k_a of unsaturated soil depends on the coupled effects of clay content and water content. Ball and Schjønning (2002) measured k_a of

soils with different clay contents at different water contents. They found that k_a of unsaturated soil decreases as soil water content increases. Moreover, k_a of soil with higher clay content would be larger or smaller than that of soil with lower clay content, depending on the water content of the two soils. Therefore, it is possible that k_a of soil with higher clay content is larger than that of soil with lower clay content in this study.

In addition, the new simple and low-cost air permeameter is able to measure k_a in an almost electricity-free way if another Marriote's bottle is used to act as a water pressure source. This potential feature makes it possible for the new air permeameter to be used in situations where financial support and electricity access are limited such as the outdoor environments (e.g., Feng et al., 2017; Cheng et al., 2018).

4. Conclusions

This study introduces a new simple and low-cost air permeameter. To verify the reliability of measurement result by this new permeameter, a comparison between k_a measured by this new air permeameter and k_a measured by the air permeameter introduced in ASTM D6539 was conducted on soil specimens with three soil textures, i.e. clay, silt loam, and sandy loam. The findings from this study are summarized as follows:

- The new air permeameter developed in this study is simple in structure and low-cost.
- The new air permeameter is able to supply steady air pressure on soil specimen and measure the flow rate of air through soil specimen accurately.
- One-way analysis of variance shows that difference of measured k_a of soil specimen between the new air permeameter and the air permeameter of ASTM D6539 is not significant (p >0.05). Thus it can be regarded that measured k_a by the new air

permeameter is reliable.

Note that although the air permeameter developed in this study can supply a steady low air pressure on soil specimens with three textures, it can be extended to a much larger air pressure supply after a few modifications are made in the further study. In addition, to take plant roots into consideration in the relevant study of root-permeated soil, accommodation for soil specimens with a larger size in this developed air permeameter needs to be further studied.

Acknowledgements

This work was supported by the Guangdong Basic and Applied Basic Research Foundation [grant number 2020B1515120083]; the National Natural Science Foundation of China [grant number 51578196 and 51808171]; the Guangdong Natural Science Foundation [grant number 2018A030310018]; the Shenzhen Key Laboratory Launching Project [grant number ZDSYS20200810113601005].

References

ASTM D6539-13, 2013. Standard test method for measurement of the permeability of unsaturated porous materials by flowing air, ASTM International, West Conshohocken, PA.

Ball, B. C., Schjønning, P. (2002). 4.4 Air Permeability. Methods of Soil Analysis: Part 4 Physical Methods, 5, 1141-1158.

Beven, K., Germann, P., 1982. Macropores and water flow in soils. Water Resour. Res., 18, 1311-1325.

Carman, P., 1956. Flow of gases through porous media. New York, NY: Academic Press.

Chen, Y., Gao, Y., Guo, H., 2021. Bio-improved hydraulic properties of sand treated

by soybean urease induced carbonate precipitation and its application Part 2: Sand-geotextile capillary barrier effect. Transp. Geotech., 27, 100484.

Chen, R., Huang, J. W., Chen, Z. K., Xu, Y., Liu, J., Ge, Y. H., 2019. Effect of root density of wheat and okra on hydraulic properties of an unsaturated compacted loam. Eur. J. Soil Sci., 70, 493-506.

Chen, R., Tan, R., Chen, Z. K., Ping, Y., Mei, Z., 2020. Influence of degree of compaction on unsaturated hydraulic properties of a compacted completely decomposed granite. Geofluids. 2020, 1-9.

Cheng, Q., Guo, H., Feng, T., Lu, Y., 2018. Volume changes of biochar-amended landfill cover soil under a thermal cycle. Waste Manage. Res., 36(12), 1223-1227.

Delage, P., Cui, Y.J., De Laure, E., 1998. Air flow through an unsaturated compacted silt. In: Proceedings of the 2nd International Conference on Unsaturated Soils, Beijing, 1, pp. 563–568.

Feng, S., Ng, C. W. W., Leung A. K., Liu, H. W., 2017. Numerical modelling of methane oxidation efficiency and coupled water-gas-heat reactive transfer in a sloping landfill cover. Waste Manage., 68: 355-368.

Gliński, J., Stępniewski, W., 1985. Soil aeration and its role for plants. Boca Raton, Florida: CRC Press, Inc..

Håkansson, I., 1990. A method for characterizing the state of compactness of the plough layer. Soil Till. Res., 16, 105-120.

Iversen, B. V., Moldrup, P., Schjønning, P., Jacobsen, O. H., 2003. Field application of a portable air permeameter to characterize spatial variability in air and water permeability. Vadose Zone J., 2, 618-626.

Kosmaras, A., 2017. Research and development of a pressure regulator. International

Hellenic University, Thessaloniki, Greece.

Li, Z. F., Wang, Y. H., Chow, J. K., Su, Z., Li, X., 2018. 3D pore network extraction in granular media by unifying the Delaunay tessellation and maximal ball methods. J. Petrol. Sci. Eng., 167, 692-701.

Meyer, C., Lüscher, P., Schulin, R., 2014. Recovery of forest soil from compaction in skid tracks planted with black alder (Alnus glutinosa (L.) Gaertn.). Soil Till. Res., 143, 7-16.

Montgomery, R. B., 1947. Viscosity and thermal conductivity of air and diffusivity of water vapor in air. J. Meteorol., 4, 193-196.

Ng, C. W. W., Chen, Z. K., Coo, J. L., Chen, R., Zhou, C., 2015a. Gas breakthrough and emission through unsaturated compacted clay in landfill final cover. Waste Manage., 44, 155-163.

Ng, C. W. W., Liu, J., Chen, R., Xu, J., 2015b. Physical and numerical modeling of an inclined three-layer (silt/gravelly sand/clay) capillary barrier cover system under extreme rainfall. Waste Manage., 38, 210-221.

Ni, J. J., Ng, C. W. W., 2019. Long-term effects of grass roots on gas permeability in unsaturated simulated landfill covers. Sci. Total Environ.**,** 666, 680-684.

Peng, K., Shi, S., Zou, Q., Zhang, Y., Tan, G., 2020. Gas permeability characteristics and energy evolution laws of gas-bearing coal under multi-level stress paths. Nat. Resour. Res., 1–22.

Qiu, Q. W., Zhan, L. T., Leung, A.K., Feng, S., Chen, Y.M., 2021. A new method and apparatus for measuring in-situ air permeability of unsaturated soil. Can. Geotech. J., 58(4): 514–530.

Rahmati, M., Neyshaboury, M. R., 2016. Soil air permeability modeling and its use for predicting unsaturated soil hydraulic conductivity. Soil Sci. Soc. Am. J., 80,

1507-1513.

Thom, R., Sivakumar, R., Sivakumar, V., Murray, E. J., Mackinnon, P., 2007. Pore size distribution of unsaturated compacted kaolin: the initial states and final states following saturation. Géotechnique, 57(5), 469-474.

USDA-NRCS., 2019. Soil texture calculator. Retrieved from https://www.nrcs.usda.gov/wps/portal/ nrcs/detail/soils/survey/

Wang, L., Liu, S., Shen, C., Lu, Y., 2021. Laboratory test and modelling of gas pressure under geomembrane subjected to the rise of groundwater in plain reservoirs. Geotext. Geomembranes, 49(1), 81-96.

Ye, W. M., Wang, C. S., Wang, Q., Chen, B., 2009. Laboratory tests on the characteristics of air-permeation in unsaturated shanghai soft soil. J. Engineering Geology. 17: 244-48. (in Chinese)

Zhan, L. T., Wu, T, Feng, S., Li, G. Y., He, H. J., Lan. J. W., Chen, Y. M., 2020. Full-scale experimental study of methane emission in a loess-gravel capillary barrier cover under different seasons. Waste Manage., 107: 54-65.

Zhan, T. L. T., Yang, Y. B., Chen, R., Ng, C. W. W., Chen, Y. M., 2014. Influence of clod size and water content on gas permeability of a compacted loess. Can. Geotech. J., 51, 1468-1474.

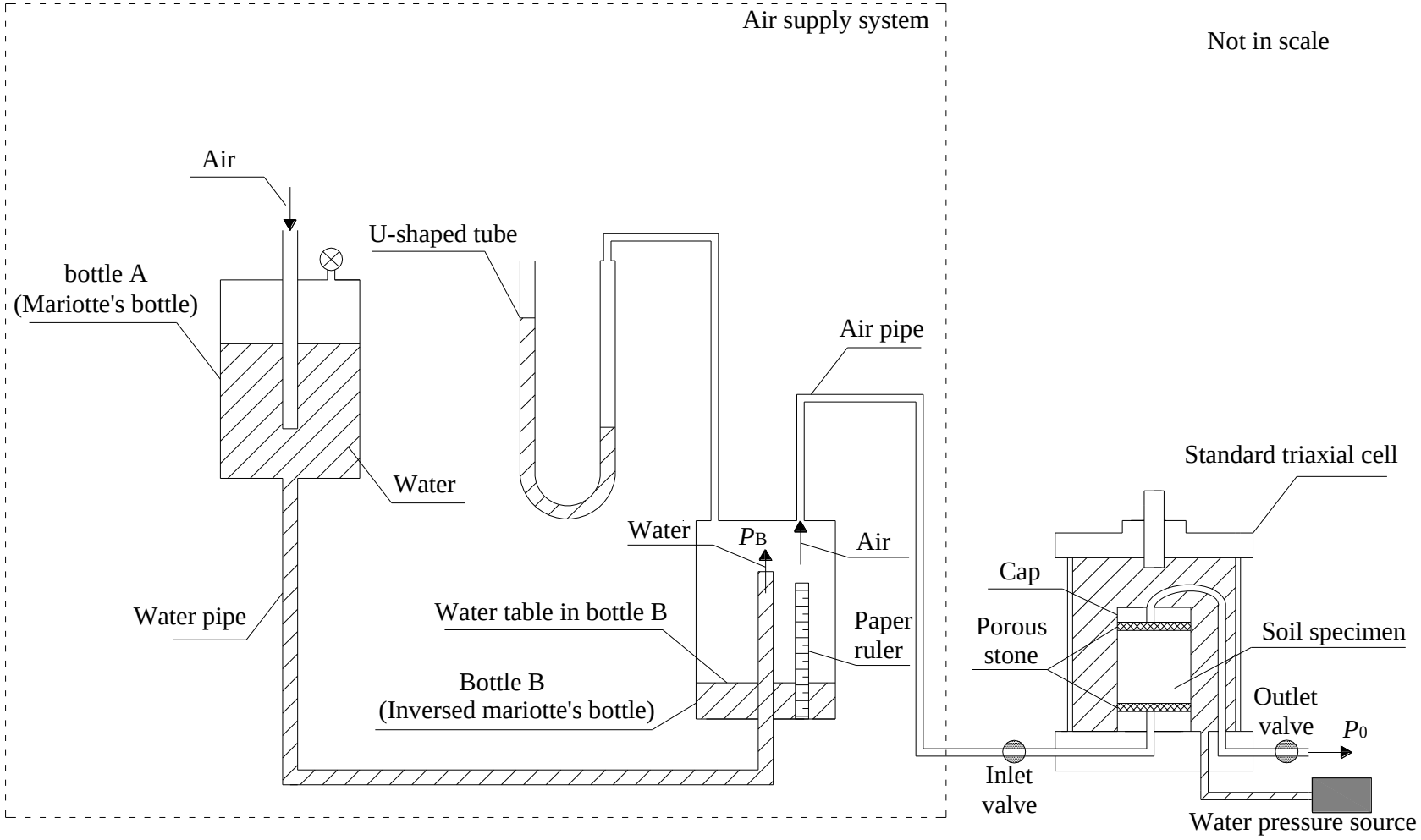

Figure 1 Schematic diagram of the newly developed air permeameter

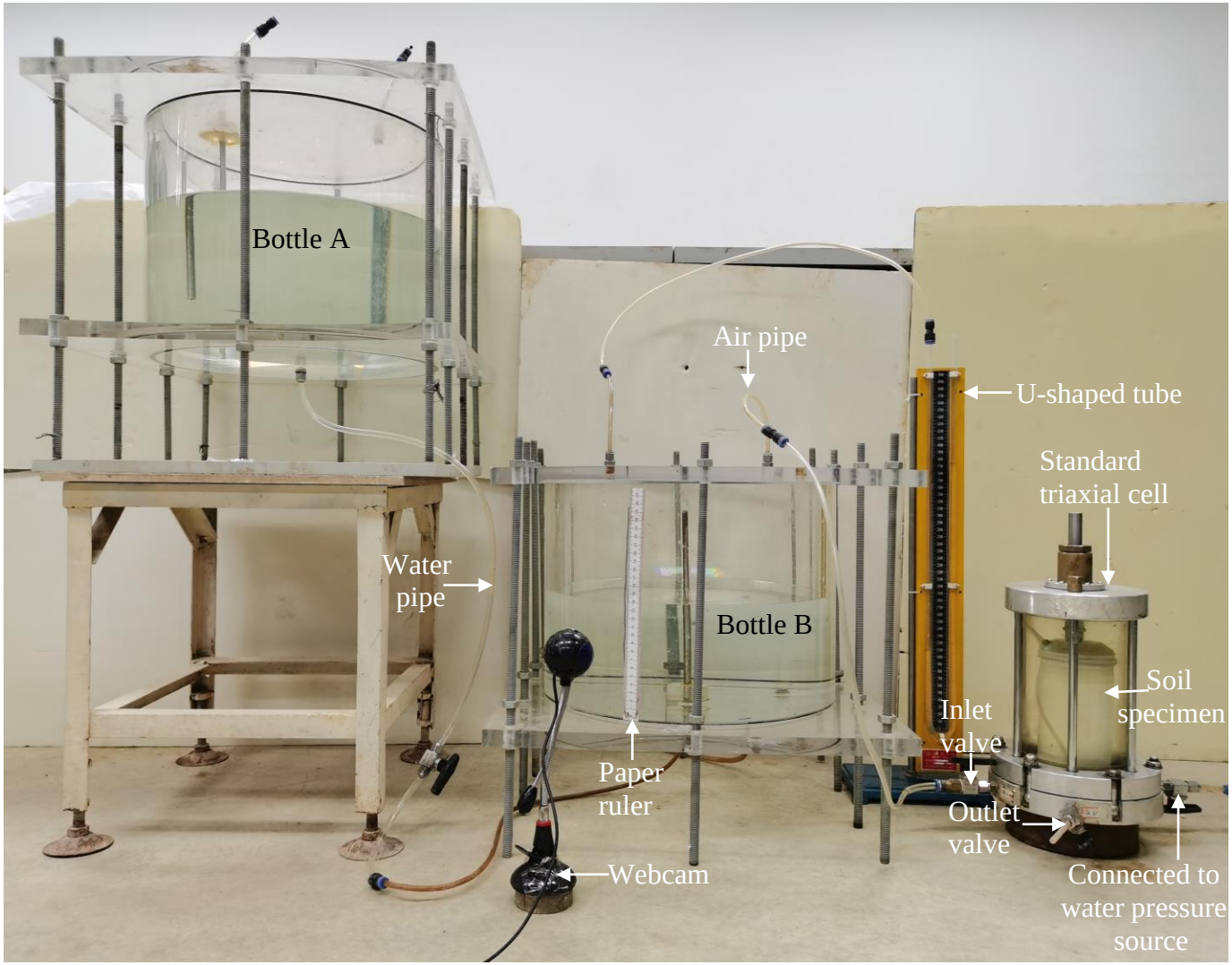

Figure 2 Photograph of the newly developed air permeameter (Color online only)

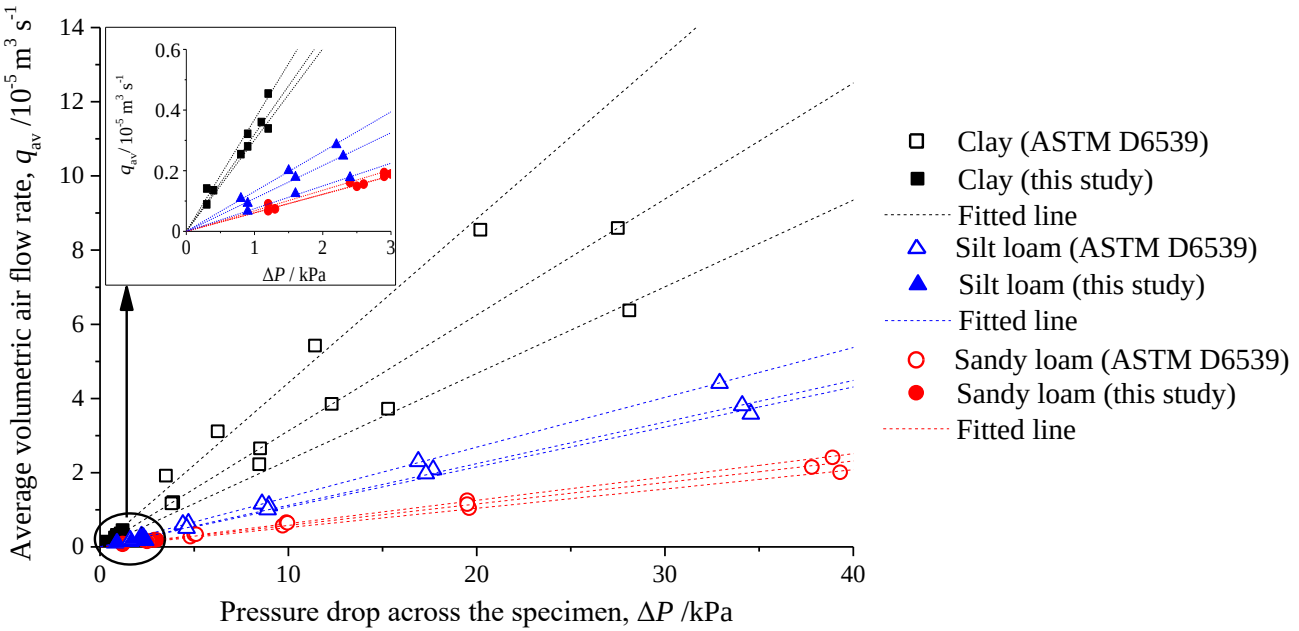

375

376 **Figure 3** Average volumetric air flow rate (q_{av}) at different values of pressure drop across the specimen (ΔP) during measurement of
377 permeability of soil specimens. Data of solid points are measured by the new air permeameter introduced in this study. Data of empty points are
378 measured by air permeameter introduced in ASTM D6539. The measured data at a lower pressure range (i.e., less than 3 kPa) is enlarged in the
379 figure.

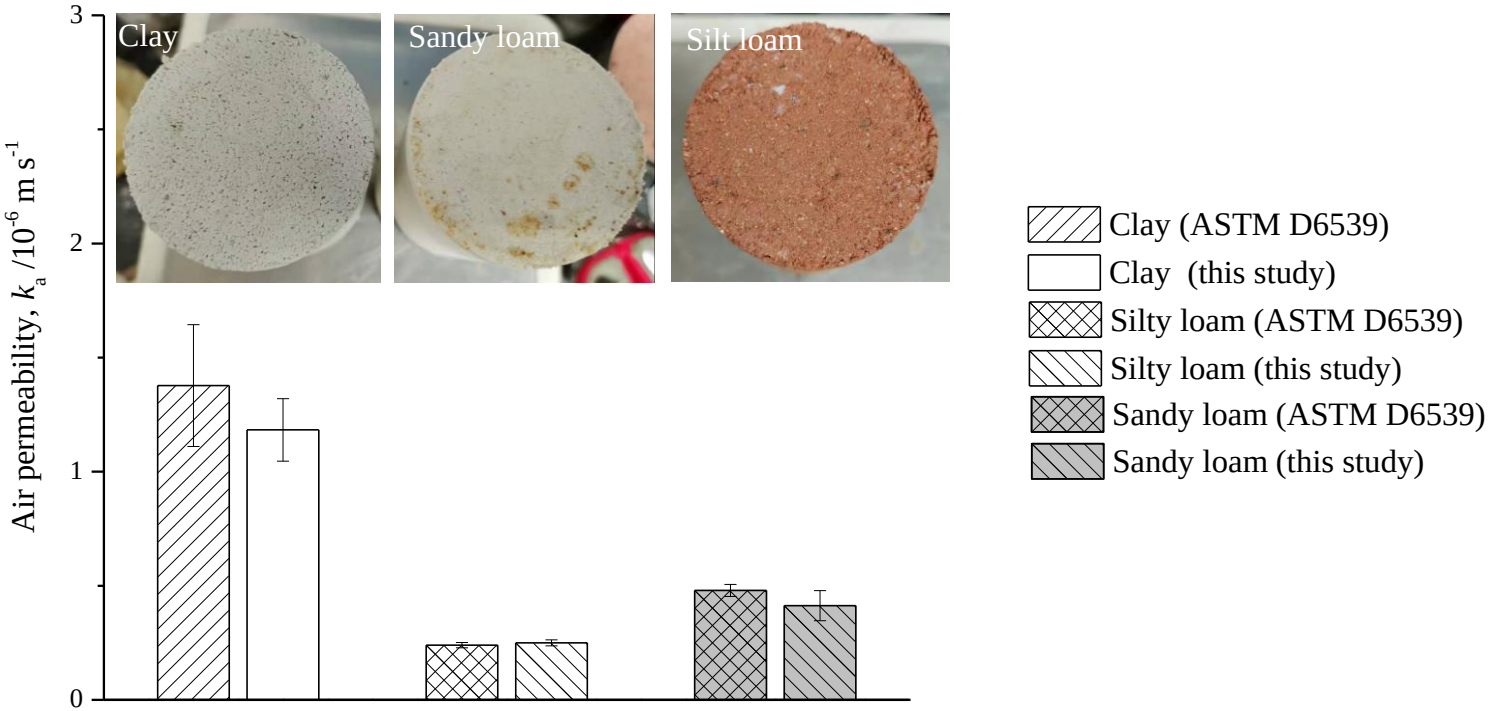

380

381 **Figure 4** Comparison of measured air permeability (k_a) of clay, silt loam, and sandy loam specimens between new permeameter introduced in
382 this study and air permeameter introduced in ASTM D6539. Error bars indicate standard errors of the three replicates. Photographs of the top
383 surface of soil specimens are shown in the figure.

Table 1 Comparison of new air permeameter of this study and air permeameter of ASTM D6539.

Air permeameter introduced in ASTM D6539	New air permeameter introduced in this study
(i) Air compressor	(i) Two Marriote's bottles
(ii) Air pressure transducer	(ii) U-shaped tube
(iii) Differential pressure transducer	(iii) Paper ruler
(iv) Custom-made tri-axial cell	(iv) Standard tri-axial cell
(v) At least two air pressure regulators	
(vi) Air flowmeter	

388 **Table 2** Basic physical properties of the soils

Gravel	Sand	Silt	Clay	Texture USDA	Optimum gravimetric water content	Maximum dry bulk density	Reference dry bulk density
%	%	%	%	-	$g\ g^{-1}$	$g\ cm^{-3}$	$g\ cm^{-3}$
32	36	28	4	Sandy loam	0.19	1.66	1.48
0	21	77	2	Silt loam	0.16	1.72	1.53
0	5	35	60	Clay	0.36	1.26	1.21

389
390

391 **Table 3** One-way analysis of variance (ANOVA) comparing measured air
392 permeability (k_a) of clay, silt loam, and sandy loam specimens between the new air
393 permeameter of this study and the air permeameter of ASTM D6539.

	Source	d.f.	Sum of squares	Mean square	*F*	*P*
k_a (clay) /10^{-14} m s^{-1}	Treatments	1	5.67	5.67	0.42	NS
	Residual	4	53.96	13.49		
	Total	5	59.62			
k_a (silt loam) /10^{-16} m s^{-1}	Treatments	1	1.48	1.48	0.32	NS
	Residual	4	18.73	4.68		
	Total	5	20.20			
k_a (sandy loam) /10^{-15} m s^{-1}	Treatments	1	6.79	6.79	0.90	NS
	Residual	4	30.22	7.56		
	Total	5	37.02			

394 d.f., degree of freedom; NS, not significant